

Wide-band and Air Dispersion Effecting the ABCD Algorithm of Phase-Recovery in Long-baseline Interferometry

Richard J. Mathar

*Leiden Observatory, Leiden University, Postbus 9513, 2300 RA Leiden, The Netherlands**

Long-baseline interferometry detects fringes created by superposition of two beams of light collected by two telescopes pointing into a common direction. The external path difference generated by pointing away from the zenith is commonly compensated by adding a variable optical path length (delay) through air for one beam such that the optical path difference between the beams remains close to zero near the detector.

The ABCD formula assigns a (wrapped) phase to the amplitudes A to D of an interference pattern shifted by multiples of 90 degrees in phase. We study the interplay between a wide band pass of the optics and the dispersion of the air in the compensating delay, which leads to small deviations between the ABCD phase and the reduced, monochromatic group-delay representation of the wave packets.

In essence, this adds dispersion to the effects that have been discussed for evacuated interferometers (telescopes in space) before [J. Opt. Soc. Am. A 22 (2005) 2774].

PACS numbers: 95.75.Kk,95.55.Br,95.85.Hp,42.30.Rx

Keywords: Optical Interferometry; Group Delay; Air Dispersion; wide band; ABCD; Astrometry

I. OVERVIEW

Angular astrometry with long-baseline interferometers is based on planar trigonometry and measures baselines and path delays. The metric of path delays may be derived with sub-wavelength resolution if the fringe amplitude is fitted to a local, monochromatic oscillation. This paper is an extended comment on the meaning of the wavelength and phase of this fit. Astronomical interferometers are generally built to accept large spectral band widths to enhance sensitivity at low light levels; the terminology of “mean” and “effective” wavelengths must be attached to well-founded statistics (integrals) over the broad-band spectra, in particular if the narrow-band concept of the group delay is used to describe the propagation of light through delay lines filled with air.

Chapter II is a tutorial on the group delay concept of waves traveling through a dispersive medium. Chapter III is a review of the role played by the fringe phase to reconstruct external path differences of star light approaching two telescopes (the long-baseline interferometer). The case of mapping the entire K band of the near infrared on a single detector channel is used as a numerical example for fringe patterns generated by a wide band pass. Chapters IV and V describe a single channel and an ABCD type of measurement of raw data and focus on the deconvolution within the data reduction process which separates spectral intensities (visibilities) from phases. Chapter VI shows examples of the variation of the pivot (mean) wave number—reduction of the mean correlated flux to a single representative spectral line—as a function of star spectral indices and atmospheric transmission.

II. WAVE PACKETS

A. Polychromatic Wave Trains

The linear superposition of two electromagnetic fields of angular frequencies $\omega_1 = v_p k_1$ and $\omega_2 = v_p k_2$ traveling at a common phase velocity v_p generates frequencies at the mean and the difference,

$$\begin{aligned} & \cos(k_1 x - \omega_1 t) + \cos(k_2 x - \omega_2 t) = \\ & \cos[k_1(x - v_p t)] + \cos[k_2(x - v_p t)] = \\ & 2 \cos \left[\frac{\omega_1 + \omega_2}{2} \left(\frac{x}{v_p} - t \right) \right] \cos \left[\frac{\omega_1 - \omega_2}{2} \left(\frac{x}{v_p} - t \right) \right] (1) \end{aligned}$$

(This is rather arbitrarily written in terms of cosines, not sines, to simplify embedding into a complex valued notation.) The combined carrier frequency $(\omega_1 + \omega_2)/2$ is close to the carrier frequency of the individual components; the new aspect is the amplitude modulation at the difference of the frequencies. Adding more waves of comparable magnitude grows a few periodic pulses at the expense of increasingly more and more of the low-frequency pulses. Figure 1 demonstrates this bunching, starting with the example of a pulse train with a spacing of 0.1 Hz for the superposition of two frequencies at 1 and 0.9 Hz. The maxima with a period of 20 s become dominant after adding 0.85 Hz, and the period of the strongest maxima is eventually stretched to 40 s as the common divisor of the frequencies becomes 0.025 Hz.

B. Group Velocity

The transition from a discrete spectrum to a continuous spectrum depletes all pulses in the wave packet; essentially one remains with a carrier frequency representing a mean of the frequencies in the wave packet,

*Electronic address: mathar@strw.leidenuniv.nl;
URL: <http://www.strw.leidenuniv.nl/~mathar>

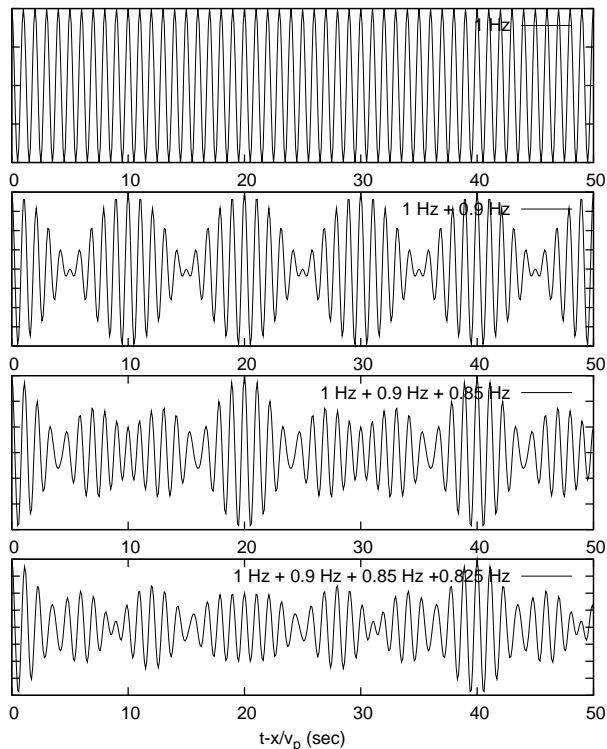


FIG. 1: Top: a monochromatic wave at 1 Hz. Second from top: a superposition of two waves of equal amplitude at 1 and 0.9 Hz. Below: the sum of three waves at 1, 0.9 and 0.85 Hz. Bottom: Four waves with differences of 0.1, 0.05 and 0.025 Hz in frequency.

and an envelope (hull) spreading inversely proportional to the width of the spectrum. The apparent velocity v_g of this wave packet is defined by virtually marking some point with amplitude $S(x, t)$ at location x and time t , waiting for a time interval Δt , and measuring by which distance Δx it has been moved:

$$S(x, t) = S(x + \Delta x, t + \Delta t). \quad (2)$$

The sum of the discrete polychromatic spectrum has become a Fourier integral for the continuous case, $S(x, t) = \int \frac{dkd\omega}{(2\pi)^2} e^{ikx - i\omega t} S(k, \omega)$. If we use the condition of stationarity, Eq. (2), in the Fourier representation,

$$\int \frac{dkd\omega}{(2\pi)^2} e^{ikx - i\omega t} S(k, \omega) = \int \frac{dkd\omega}{(2\pi)^2} e^{ikx - i\omega t} e^{ik\Delta x} e^{-i\omega\Delta t} S(k, \omega), \quad (3)$$

we may expand $S(k, \omega)$ in the exponentials around pivot values k_0 and ω_0 representative of the center of the spectrum,

$$e^{ik\Delta x - i\omega\Delta t} \approx e^{ik_0\Delta x - i\omega_0\Delta t} \times [1 + i(k - k_0)\Delta x - i(\omega - \omega_0)\Delta t + \dots] \quad (4)$$

The leading term in this expansion ensures that (3) is valid to the order that does not depend on Δx and Δt .

The group velocity is defined as the “observed” motion $v_g \equiv \lim_{\Delta t \rightarrow 0} \Delta x / \Delta t$. To fulfill (4) also to the linear order $O(\Delta x, \Delta t)$, the eliminating constraint becomes

$$i(k - k_0)\Delta x - i(\omega - \omega_0)\Delta t = 0. \quad (5)$$

Division through $i\Delta t$ and $i(k - k_0)$ means [28][9, §1.3.4]

$$v_g = \frac{\omega - \omega_0}{k - k_0} \equiv \frac{\partial \omega}{\partial k}. \quad (6)$$

The transition from the quotient to the differential implies that the band width is small in the sense that (i) the additional variation of $S(k, \omega)$ in the kernel of (3) is negligible, and (ii) the second and higher order derivatives of the eigenmodes $\omega(k)$ are also negligible.

C. Group Refractive Index

The microscopic absorption and emission processes of an electromagnetic wave passing through gaseous or condensed matter can be summarized as a wavelength dependent refractive index $n(k, \omega)$; in the long-wavelength limit—i.e., $\lambda \equiv 2\pi/k$ much larger than the inter-molecular distance or lattice unit cell—the superposition of many of these elementary processes replaces the vacuum wavelength by eigenmodes of the dispersion

$$ck = n(k, \omega)\omega. \quad (7)$$

Division through kn replaces the vacuum phase velocity c by the phase velocity

$$v_p \equiv \frac{c}{n} = \frac{\omega}{k}. \quad (8)$$

The concept of the group refractive index transforms this pair of variables v_p and n further to a pair of variables v_g and n_g to acknowledge that the relevant speed of fringe packets switches from v_p to v_g : If the setup is concerned with moving them through different geometric paths and monitoring a high coherent signal at a detector position, the geometric path lengths must involve v_g to synchronize the times of arrival to achieve interference near the detector. To switch from (v_p, n) to (v_g, n_g) , (8) is rewritten to define the group refractive index n_g ,

$$v_g \equiv \frac{c}{n_g}. \quad (9)$$

The derivative of (7) w.r.t. k is with (6)

$$c = \frac{\partial n}{\partial k} \omega + n \frac{\partial \omega}{\partial k} = \frac{\partial n}{\partial k} \frac{ck}{n} + nv_g. \quad (10)$$

This equation is solved for v_g and inserted into (9),

$$n_g = \frac{c}{v_g} = \frac{c}{\frac{c}{n} - \frac{\partial n}{\partial k} \frac{ck}{n^2}} = \frac{n}{1 - \frac{\partial n}{\partial k} \frac{k}{n}}. \quad (11)$$

This equation is accurate, see Eqs. (4)–(5) in [16] and Eq. (3) in [19]. Assuming weak dispersion, its geometric

series expansion in powers of the small $\partial n/\partial k$ may be truncated after the linear term:

$$n_g \approx n \left(1 + \frac{\partial n}{\partial k} \frac{k}{n} \right) = n + k \frac{\partial n}{\partial k}, \quad (12)$$

which is the version in [12, p. 1666] and [38, p. 768]. The relative error in (12) is approximately the first neglected order, $(\frac{\partial n}{\partial k} \frac{k}{n})^2 = (\frac{\partial n}{\partial \sigma} \frac{\sigma}{n})^2$ where $\sigma = k/(2\pi) = 1/\lambda$ is the spectroscopic wave-number. In the K band around $\sigma \approx 4400 \text{ cm}^{-1}$ at air pressures around 750 hPa, a typical value is $\partial n/\partial \sigma \approx 1.2 \times 10^{-10} \text{ cm}$, which yields a relative error $\approx 2 \times 10^{-13}$. In the N band [13, 21, 22, 30], the relative error would still be tiny.

A short-hand with one (and more) primes as in

$$n'(k) = \partial n/\partial k \quad (13)$$

will subsequently be used to represent the first (and higher) order derivatives w.r.t. k .

D. Time Delay

A group delay t_g is implicitly defined via (5) as the time Δt for a *fixed* Δx . Again in the limit of small deviations from a reference (k_0, ω_0) , this becomes

$$t_g \equiv \Delta x \frac{\partial k}{\partial \omega}. \quad (14)$$

The derivative of (8), $k = \omega/v_p$, with respect to ω is $\partial k/\partial \omega = 1/v_p - (\omega/v_p^2)(\partial v_p/\partial \omega)$ and inserted, using $t = \Delta x/v_p$ for the un-dispersed reference time delay,

$$t_g = \Delta x \frac{1}{v_p} - \Delta x \frac{\omega}{v_p^2} \frac{\partial v_p}{\partial \omega} = t - \omega \frac{t}{v_p} \frac{\partial v_p}{\partial \omega}. \quad (15)$$

At fixed Δx , the total differential of $x = tv_p$ must remain zero, $tdv_p + v_p dt = 0$, which is used to substitute $t \partial v_p \rightsquigarrow -v_p \partial t$ in (15) and to recover the Meisner formula [34]

$$t_g = t + \omega \frac{\partial t}{\partial \omega}. \quad (16)$$

III. SYNTHETIC BROAD-BAND FRINGES

A. Model Air Dispersion

In the numerical examples that follow, a model of the refractive index n in the near-infrared is needed. It is demonstrated in Fig. 2 calculated from an update of an oscillator strength summation [30]. Since we also employ integrations over the dispersion spectrum, it is favorable to replace this detailed spectrum by a fit, explicitly

$$n - 1 = \sum_{i=0,1,\dots} c_i(T, p, H) (\sigma - \sigma_{\text{ref}})^i; \quad (17)$$

$$c_i(T, p, H) = c_{i\text{ref}} + c_{iT} \left(\frac{1}{T} - \frac{1}{T_{\text{ref}}} \right) + c_{iH} (H - H_{\text{ref}}) + c_{ip} (p - p_{\text{ref}}). \quad (18)$$

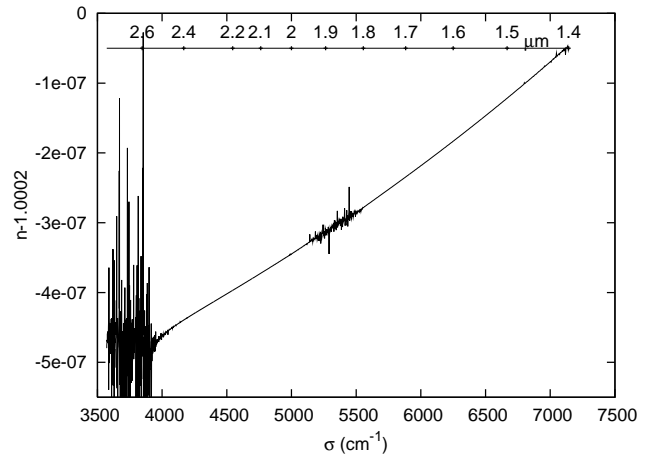


FIG. 2: A prototypical infrared dispersion of humid air at $p = 744 \text{ hPa}$, $T = 16 \text{ }^\circ\text{C}$ and 10% humidity in the K band around 4500 and the H band around 6500 cm^{-1} .

Here, T is the absolute temperature with a reference value of T_{ref} , p is the air pressure with a reference value set at p_{ref} , H the relative humidity between 0 and 100 with a reference value set at H_{ref} , σ is the wave-number with a reference value set at σ_{ref} , and c_i are the expansion coefficients of Table I.

i	$c_{i\text{ref}} / \text{cm}^i$	$c_{iT} / [\text{cm}^i \text{K}]$
0	0.000199594	0.0583358
1	0.113225×10^{-9}	-0.330288×10^{-7}
2	$-0.438053 \times 10^{-14}$	0.811015×10^{-10}
3	0.101921×10^{-16}	$-0.514801 \times 10^{-13}$
4	$-0.296872 \times 10^{-20}$	0.150602×10^{-16}
5	0.311755×10^{-24}	$-0.157482 \times 10^{-20}$
i	$c_{iH} / [\text{cm}^i \text{ \%}]$	$c_{ip} / [\text{cm}^i \text{ Pa}]$
0	-0.904550×10^{-8}	0.268437×10^{-8}
1	0.119196×10^{-11}	0.136651×10^{-14}
2	$-0.149163 \times 10^{-14}$	0.136002×10^{-18}
3	0.985685×10^{-18}	0.822304×10^{-23}
4	$-0.288288 \times 10^{-21}$	$-0.224090 \times 10^{-26}$
5	0.301528×10^{-25}	0.251260×10^{-30}

TABLE I: Fitting coefficients for the multivariate Taylor expansion (18) to the real part of the index of refraction for $T_{\text{ref}} = (273.15 + 16) \text{ K}$, $p_{\text{ref}} = 74400 \text{ Pa}$, $H_{\text{ref}} = 10 \text{ \%}$, $\sigma_{\text{ref}} = 1/(2.25 \mu\text{m}) = 4444.4 \text{ cm}^{-1}$, $1.3 \mu\text{m} \leq 1/\sigma \leq 2.5 \mu\text{m}$.

The coefficient c_{0T} means a change of the temperature by $\Delta T = 1 \text{ K}$ changes $\Delta \frac{1}{T} = -\frac{\Delta T}{T^2}$ by 10^{-5} K^{-1} , changes n by 6×10^{-7} and relocates the wave packet by $60 \mu\text{m}$ after a path of 100 m if $\lambda = 2.25 \mu\text{m}$. The coefficient c_{0H} means a change of the relative humidity by 10 percent points changes n by 0.9×10^{-7} and relocates the packet by $9 \mu\text{m}$ over the same path at the same wavelength. Introducing the fit replaces Fig. 2 by Fig. 3.

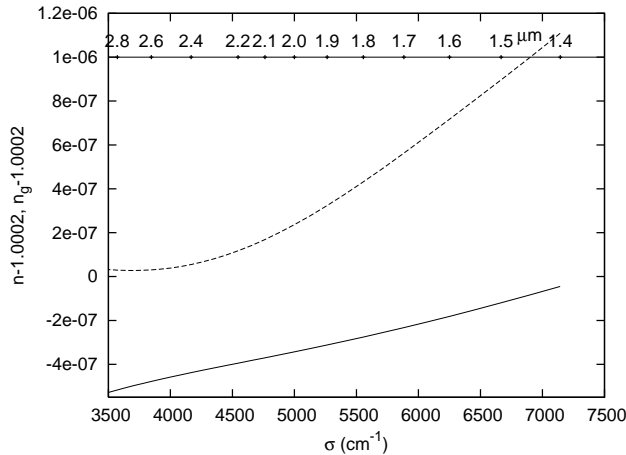


FIG. 3: The lower line is n fitted to Fig. 2 according to (18); the upper line is $n_g = n + n'k$ derived from this fit according to (12).

B. Model of Two-beam Interference

Illuminated by a source with coherent spectral energy density $e(k)$, the superposition of the light with a second beam forced to a detour of a compensating geometric path length D_i yields a fringe pattern

$$A(D_i) = \int e(k) \{1 + \cos[n(k)kD_i - kD_e]\} dk, \quad (19)$$

assuming no correlation between the fields (amplitudes) at different k . D_e is the (vacuum) delay imprinted on the two beams at arrival of the two telescopes, essentially the dot product between the baseline vector and a unit vector into the pointing direction [7]. (The wavelength dependence of D_e from lensing effects by the atmosphere above the telescopes [8, 29, 31] and piston fluctuations are ignored here.)

D_i is the “internal” geometric path difference added by the mirror train on the ground, and nD_i the associated optical path difference, which is controlled as to steer the phase of the cosine to some desired value in some average sense. The coherent flux $e(k)$ is the one experienced by the detector which produces the signal A [43]: it is the product of (i) the star emission, by (ii) the Earth’s sky transmission [17], by (iii) the reflectivity of mirror optics and transmissivity of beam combiner optics, including vibrations and diffraction effects [40], and by (iv) the coupling efficiency of any fiber optics and quantum efficiency of the detector, including tilt effects [2, 4]. We will represent the star emission by black body spectra of Fig. 4, the sky transmission by the model of Fig. 5, ignore chromaticism of the transmission of intermediate optics and use the quantum efficiency of Fig. 6.

A different approach to delay compensation establishes the term nD_i with a dispersion compensator [6, 26, 45]. This trades the variability of the air dispersion [21] by the dependence of the glass dispersion on temperature

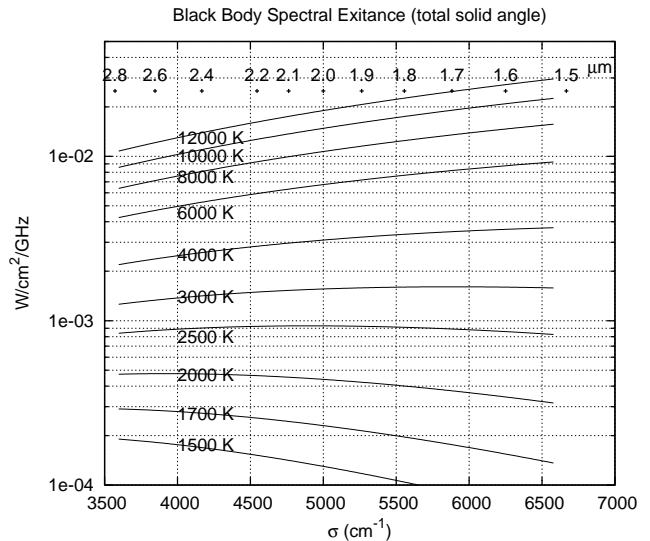


FIG. 4: Black body spectral densities $2\pi h\nu^3/[c^2(e^{h\nu/k_B T} - 1)]$ between 1.52 and 2.78 μm on a semi-logarithmic scale, where h are the Planck and k_B the Boltzmann constant.

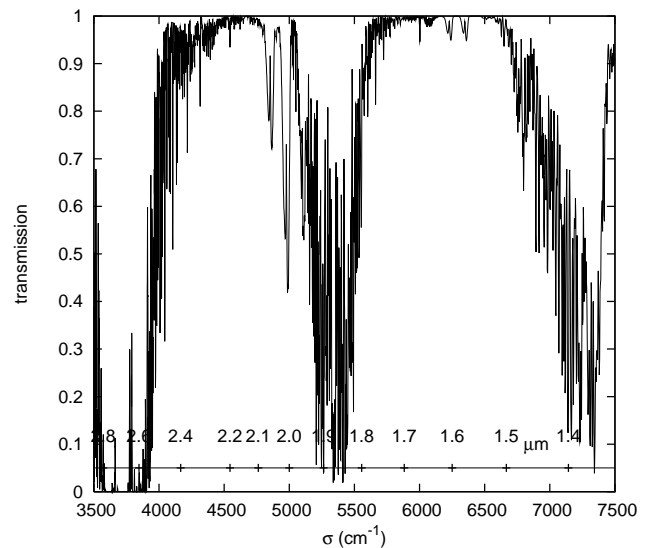


FIG. 5: Synthetic Mauna Kea sky transmission in the K band at an airmass of 1.0 and a 1.6 mm water vapor column [27].

and expansion coefficients [10] and is not discussed here.

As a model of the band pass [specification of the integration interval in (19)] we will use parameters that follow from placing an Infrasil [20] prism of a wedge angle of 11.9° in front of the detector, and reverse interpolation of the formula of the refraction angle [9, 18][9, §4.7.2]. An extreme setup in terms of band pass width would map the entire K band from 2.05 to 2.45 μm onto a single detector pixel with output A . The non-linearity of the prism equation and prism material dispersion would map most of the H band onto one of the side channels,

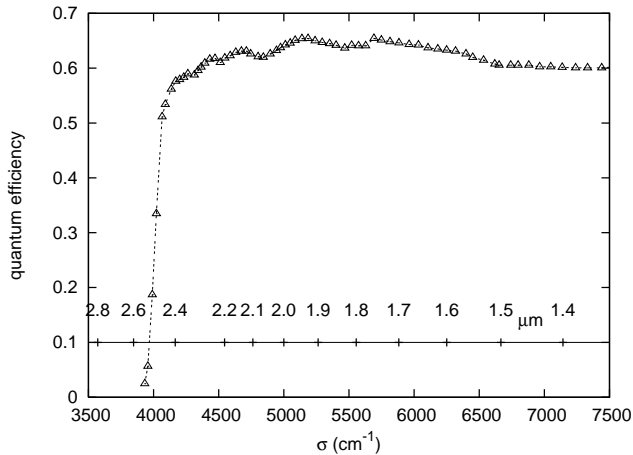


FIG. 6: Quantum efficiency of the 256×256 Rockwell PIC-NIC detector.

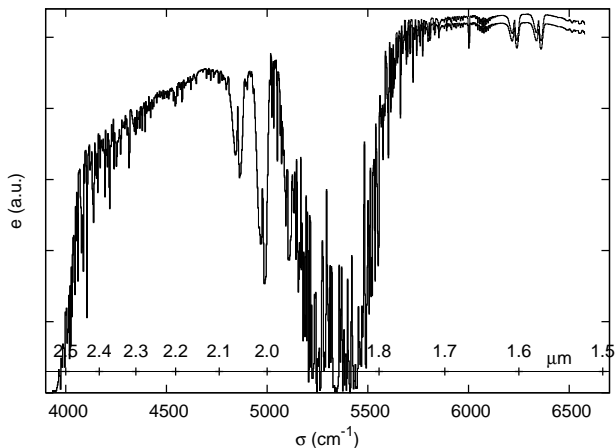


FIG. 7: Prototypical model of $e(k)$ constructed as a product of Fig. 5, Fig. 6 and a black body of 8000 K or 9000 K.

as summarized in Table II.

The main advantage of wide-band detection is the increase of the signal A given limited intensity e and noise by photon noise, detector readout and thermal background. The focus of this work here is to point at some inherent disadvantages.

C. Delay Tracking

The philosophy of coherencing is to actuate the delay line (DL), the variable D_i , to manipulate the phase difference

$$\varphi(k) = nkD_i - kD_e \quad (20)$$

in (19). Tracking on a local maximum (peak) of A would try to achieve a broad maximum or minimum of φ as a function of k , since the nearby spectral elements of $e(k)$ then all add up “in phase.” The difference between

wedge (°)	incid. (°)	# pixels	limits (μm)			
11.9	8.4522	3	1.52	2.05	2.45	2.78
22.59	10.0084	2	2.05	2.26	2.45	
31.7	14.3783	3	2.05	2.19	2.32	2.45
39.04	18.173	4	2.05	2.15	2.25	2.35 2.45

TABLE II: The spectral range of detector pixels if the wedge angle of the prism is increased for higher dispersion, and the incidence angle is chosen to stay with a minimum total deflection angle between the direction of incidence and the direction of exit. The calculations are for Infrasil assuming that each pixel is equivalent to 0.0014077 rad difference in the exit angles.

nulling the phase and this coherencing is symbolized by the difference between Fig. 8 and Fig. 9: Setting D_i to

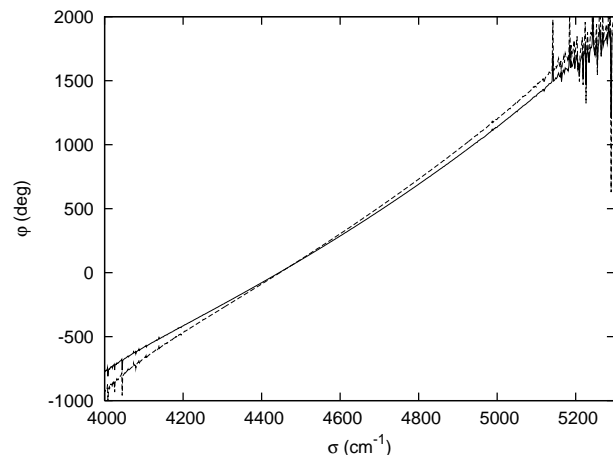


FIG. 8: The residual phase $\varphi(k)$ for a geometric delay $D_e = 100$ m as a function of $\sigma = k/(2\pi)$: The solid line is for 10% humidity at 744 hPa, 16°C and $D_i = 99.980\,044\,790$ m. The dashed line for 20% humidity at the same pressure and temperature and $D_i = 99.980\,053\,689$ m. The D_i are chosen as to achieve a common zero at $\lambda = 2.25$ μm ($\sigma = 4444$ cm^{-1}); the 9 μm difference between the D_i corresponds to c_{0H} of Table I.

steer $\varphi(k)$ close to zero as in Fig. 8 accumulates phases in the integral (19) that differ by a few hundred degrees if $e(k)$ covers a broad range of the spectrum. To achieve less chaotic/oscillatory behavior of the integrand, one would move D_i to achieve a flatter $\varphi(k)$ to reach Fig. 9 (see [46] for N band examples). The spectral elements in a small interval of similar $\varphi(k)$ interfere positively. The extremum of $\varphi(k)$ pinpoints the “effective” wave-number because the populated density of φ -states is largest there. Mathematically speaking, the extremum is characterized by a vanishing derivative of (20),

$$\frac{\partial \varphi}{\partial k} = n'kD_i + nD_i - D_e = 0. \quad (21)$$

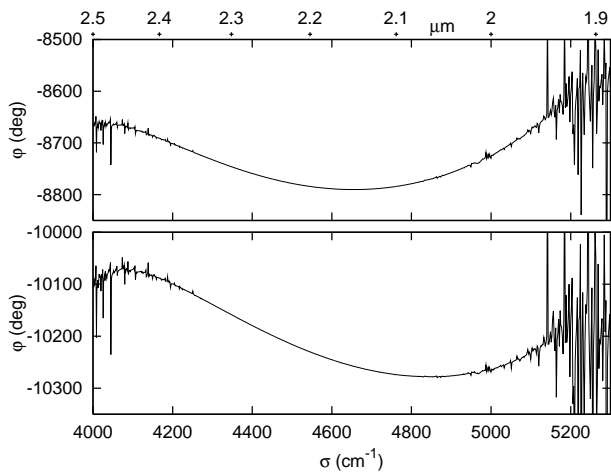


FIG. 9: The phase φ of (20) for a geometric delay $D_e = 100$ m as a function of wave-number: The upper plot is for 10% humidity at 744 hPa, 16 °C and $D_i = 99.97999$ m. The lower plot for 20% humidity at the same pressure, temperature and D_i .

Solving this for the geometric compensating path D_i with (12) yields

$$D_i = D_e/n_g. \quad (22)$$

This verifies the claim of Section II C that n_g is the scale factor to replace n in the realm of fringe tracking. In the limit of constant $n_g(k)$ and $n(k)$, the fringe pattern A of (19) is an ordinary Fourier Cosine Transform of the source spectrum $e(k)$, its Michelson interferogram.

Apart from a sign flip and scaling with D_e , Fig. 9 is equivalent to the upper part of [16, Fig 1]: Their fringe tracking selects a minimum of Fig. 9 by moving D_i , then chooses another (but unique) φ_{gui} in the two adjacent spectral channels to define “guiding” wave-numbers. However, Fig. 9 points at a prospective problem with large band passes: such a pair of wave-numbers may not exist in the two neighboring channels when nonlinear dispersion, i.e., $n''(k) \neq 0$, may create a non-parabolic shape of $\varphi(k)$ such that no two solutions to $\varphi(k) = \varphi_{\text{gui}}$ may exist due to the additional extremum.

D. Numerical Examples

Fig. 10 and 11 show examples of the interplay of the 8000 K spectrum of Fig. 7 with the dispersion of Fig. 3, integrated over three adjacent intervals as specified by the first line of Table II. The middle plot illustrates how the deep cut in the spectrum from 1.8 to 1.9 μ initiates a break-up of the main envelope into fragments in some sort of restoration of the multiple packets scheme that was the foundation of Fig. 1.

The roughest estimate of the position D_i of the fringe center—ignoring the effect of the weighting with the star color $e(k)$ —is where the argument of the cosine of Eq.

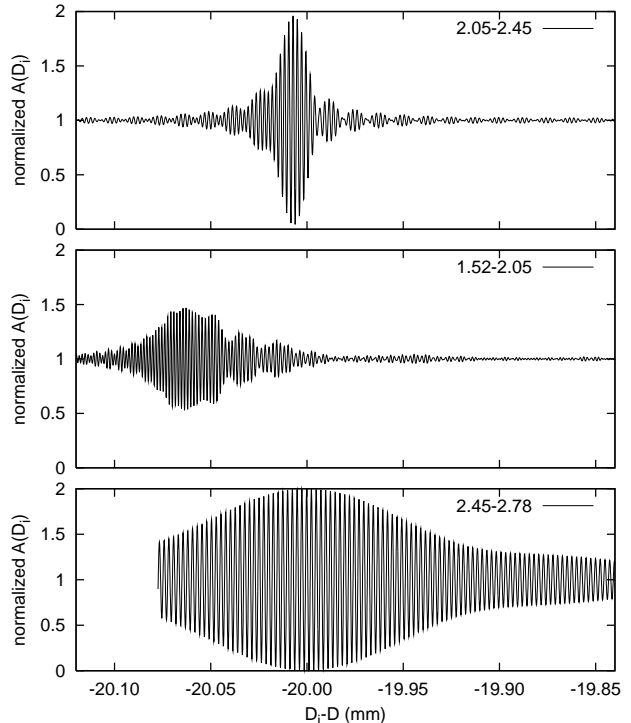


FIG. 10: Normalized K band fringe $A(D_i)/e_0$ according to Eq. (19) for the 8000 K spectrum of Fig. 7 for the three bands of the first line in Table II at an external delay of $D_e = 100$ m, including nonlinear air dispersion $n(k)$.

(19) becomes zero. If one assumes a constant refractive index $n(\bar{k})$ inside the band, this is

$$D_i = D_e/n(\bar{k}). \quad (23)$$

The relative error of this formula in comparison with the more accurate (22) is $n_g(\bar{k}) - n(\bar{k})$, typically the distance of 4×10^{-7} between the curves in Fig. 3.

IV. BEYOND THE GROUP DELAY APPROXIMATION

A. Moment Expansion

1. Nonlinear Dispersion

Up to here, we have focused on the dispersion $n(k)$ as the key parameter to locate the fringe packet. In practise, the “astrometric” interpretation of the interferometric datum A is concerned with the recovery of the external delay D_e given A and D_i as the raw data. (In contrast to the “imaging” experiment which tries to measure the magnitude of A as a function of D_e , this quest is complementary as it aims at determining *where* on the D_e axis the zero optical path difference is, rather than determining the degree of coherence that would represent the star’s brightness distribution.) The key subject

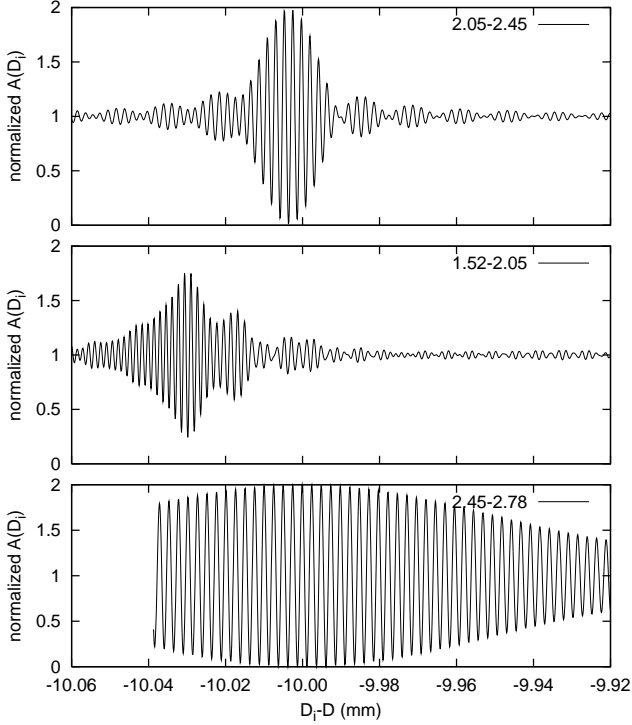


FIG. 11: The calculations of Fig. 10 repeated for a vacuum delay of $D_e = 50$ m.

of this paper is the additional role of the spectrum $e(k)$ and its interplay with the dispersion when the weighting with the correlated flux lets the “observed” phase of $A(D_i)$ deviate from the “guiding” phase of an extremum of $\varphi(k)$.

To understand this phenomenon, one introduces a Taylor expansion of the dispersion expansion around some “central” value \bar{k} in the spirit of Filon quadratures [23],

$$n(k) = n(\bar{k}) + (k - \bar{k})n'(\bar{k}) + \frac{(k - \bar{k})^2}{2}n''(\bar{k}) + \frac{(k - \bar{k})^3}{6}n'''(\bar{k}) + \dots \quad (24)$$

Higher order derivatives are

$$n_g(\bar{k}) \equiv n(\bar{k}) + \bar{k}n'(\bar{k}), \quad (25)$$

$$n'_g(\bar{k}) \equiv \frac{\partial n_g}{\partial k} \Big|_{\bar{k}} = 2n'(\bar{k}) + \bar{k}n''(\bar{k}), \quad (26)$$

$$n''_g(\bar{k}) = 3n''(\bar{k}) + \bar{k}n'''(\bar{k}). \quad (27)$$

Quick calculations use Table I:

$$n'_g = \frac{1}{2\pi} \left(2 \frac{dn}{d\sigma} + \sigma \frac{d^2n}{d\sigma^2} \right) \quad (28)$$

evaluated at σ_{ref} is

$$n'_g = \frac{1}{2\pi} (2c_{1\text{ref}} + 2\sigma_{\text{ref}}c_{2\text{ref}})$$

$$= \frac{1}{\pi} (0.113225 \times 10^{-9} - 4444 \times 0.438 \times 10^{-14}) \text{cm} \approx 3.0 \times 10^{-13} \text{m}, \quad (29)$$

for example. Equivalent expansion of $e(k)$ defines the moments of the energy spectrum,

$$e_m \equiv \int e(k)(k - \bar{k})^m dk \quad (30)$$

around any chosen center \bar{k} [47]. For pure black body spectra, e_m is a binomial sum over Debye functions up to order $3 + m$ [1, §27.1].

2. Asymmetric Coherent Spectra

Eq. (19) is accordingly expanded up to third order in $k - \bar{k}$,

$$\begin{aligned} A(D_i) &\approx \{1 + \cos[n(\bar{k})\bar{k}D_i - \bar{k}D_e]\} e_0 \\ &- \{[n'(\bar{k})\bar{k} + n(\bar{k})]D_i - D_e\} \sin[n(\bar{k})\bar{k}D_i - \bar{k}D_e] e_1 \\ &- \frac{1}{2} \{[n'(\bar{k})\bar{k} + n(\bar{k})]D_i - D_e\}^2 \cos[n(\bar{k})\bar{k}D_i - \bar{k}D_e] e_2 \\ &- \frac{1}{2} [n''(\bar{k})\bar{k} + 2n'(\bar{k})] D_i \sin[n(\bar{k})\bar{k}D_i - \bar{k}D_e] e_2 \\ &- \frac{1}{2} \{[n'(\bar{k})\bar{k} + n(\bar{k})]D_i - D_e\} [n'(\bar{k})\bar{k} + 2n'(\bar{k})] \\ &\quad \times D_i \cos[n(\bar{k})\bar{k}D_i - \bar{k}D_e] e_3 \\ &+ \frac{1}{6} \{[n'(\bar{k})\bar{k} + n(\bar{k})]D_i - D_e\}^3 \sin[n(\bar{k})\bar{k}D_i - \bar{k}D_e] e_3 \\ &- \frac{1}{6} [n'''(\bar{k})\bar{k} + 3n''(\bar{k})] D_i \sin[n(\bar{k})\bar{k}D_i - \bar{k}D_e] e_3 + O(e_4) \beta 1 \\ &\approx [1 + \cos \varphi(\bar{k})] e_0 - [n_g(\bar{k})D_i - D_e] e_1 \sin \varphi(\bar{k}) \\ &- \frac{1}{2} [n_g(\bar{k})D_i - D_e]^2 e_2 \cos \varphi(\bar{k}) \\ &- \frac{1}{2} n'_g(\bar{k}) D_i e_2 \sin \varphi(\bar{k}) \\ &- \frac{1}{2} [n_g(\bar{k})D_i - D_e] n'_g(\bar{k}) D_i e_3 \cos \varphi(\bar{k}) \\ &+ \frac{1}{6} [n_g(\bar{k})D_i - D_e]^3 e_3 \sin \varphi(\bar{k}) \\ &- \frac{1}{6} n''_g(\bar{k}) D_i e_3 \sin \varphi(\bar{k}) + O(e_4). \quad (32) \end{aligned}$$

If we gather cosine and sine coefficients in the form

$$A = e_0 + C \cos \varphi(\bar{k}) - S \sin \varphi(\bar{k}) \quad (33)$$

with

$$\begin{aligned} C &\equiv e_0 - \frac{1}{2} [n_g(\bar{k})D_i - D_e]^2 e_2 \\ &- \frac{1}{2} [n_g(\bar{k})D_i - D_e] n'_g(\bar{k}) D_i e_3 + \dots, \quad (34) \end{aligned}$$

$$\begin{aligned} S &\equiv [n_g(\bar{k})D_i - D_e] e_1 + \frac{1}{2} n'_g(\bar{k}) D_i e_2 \\ &- \frac{1}{6} [n_g(\bar{k})D_i - D_e]^3 e_3 + \frac{1}{6} n''_g(\bar{k}) D_i e_3 + \dots \quad (35) \end{aligned}$$

the fringe packet is cast into a monochromatic format,

$$A = e_0 + \sqrt{C^2 + S^2} \cos[\varphi(\bar{k}) + \varphi_i], \quad (36)$$

and rigorously defines an “observed” phase $\varphi(\bar{k}) + \varphi_i$,

$$\tan \varphi_i = S/C. \quad (37)$$

3. Remark on Nomenclature

The standard use of the word “dispersion” in the realm of refractive indices is the prismatic dispersion due to $n'(k) \neq 0$. Linear dispersion may then describe a linear relation between the refractive index and wavelength (called *first order dispersion* in [33, 34]) or between refractive index and wave-number. For the theory described here, we will obviously use the latter, also keeping in mind that a Sellmeier functional description near resonances of Lorentzian shape would support this assumption. The goodness of fit of the actual air refractive index to either $\partial n/\partial \lambda \approx \text{const}$ or $\partial n/\partial k \approx \text{const}$ is coincidental: whereas Fig. 2 indicates that $\partial n/\partial k$ is approximately constant in the K band, the equivalent plots at longer infrared regions are more complicated, see Fig. 12.

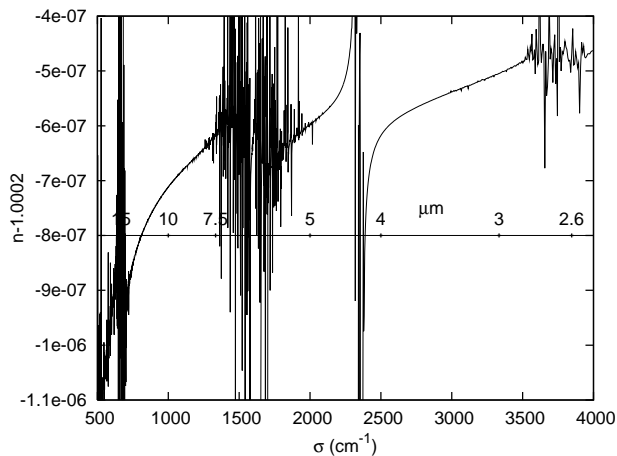


FIG. 12: The continuation of Fig. 3 into the mid-infrared.

For the wave packet analysis, the focus shifts from $n(k)$ to $n_g(k)$ and its derivatives. Eq. (26) proves that a linear dispersion in the sense of $n''(k) = 0$ induces a linear dispersion $n_g''(k) = 0$ at the same k . However, Fig. 3 demonstrates that the nonlinearity of n_g has a tendency of being stronger than the nonlinearity of n , inherited from the admixture of higher derivatives of n in the last terms of Eqs. (25)–(27). The curves of constant group delay $n_g'(k) = 0$ are of the form $n(k) = f/k + n_\infty$ with constants f and n_∞ , which means they need linearity between n and λ .

B. Effective Wave-number

1. Choice

The fringe packet lives at the DL position D_i where the amplitude $(C^2 + S^2)^{1/2}$ of (36) is maximum, which means C and S should have no linear terms in the vicinity. The dominating non-constant term $\propto e_2$ in (34) has already a quadratic form. The dominating leading term $\propto e_1$ in (35) has a linear component in D_i ; from there we may summarize the rationale of group delay tracking:

- enforce

$$e_1 = 0 \quad (38)$$

by choosing

$$\bar{k} = \frac{\int k e(k) dk}{\int e(k) dk} = 2\pi \bar{\sigma} \quad (39)$$

as the effective center of the band, then

- set D_i according to (22) such that the value of C falls off quadratically from e_0 ; the factor in front of the term $\propto e_3$ of (34) and the cubic factor in one of the terms $\propto e_3$ of (35) become zero.

As a by-product, the term $\propto S$ becomes small. With (37), φ_i becomes close to zero, and the remaining oscillation $\propto \cos \varphi(\bar{k})$ show that the definition (39) has indeed picked up the very point \bar{k} of the spectrum where the phase φ calculated from n assumes the value of the entire wave packet represented by n_g . The distances between the lobes are characterized by $\Delta \varphi(\bar{k}) = 2\pi$ which implies $\Delta D_i = 1/[\bar{\sigma} n(\bar{\sigma})]$.

In this approximation, the fringe envelope in (36) is $\sqrt{C^2 + S^2} \approx C \approx e_0 - \frac{1}{2}(n_g D_i - D_e)^2 e_2$, which recovers a well-known estimate for the package width: The half width at half maximum is defined as C drops from e_0 to $e_0/2$, which happens at $(n_g D_i - D_e)^2 = e_0/e_2$. Therefore

$$D_i^{\text{FWHM}} = 2\sqrt{e_0/e_2} \quad (40)$$

is the full width at half maximum. If the spectrum is flat over its full width k^{FW} , $e(k) = I$ for $|k - \bar{k}| \leq k^{\text{FW}}/2$, the moments are $e_0 = I k^{\text{FW}}$ and $e_2 = I \int_{-k^{\text{FW}}/2}^{k^{\text{FW}}/2} k^2 dk = I (k^{\text{FW}})^3/12$ to give

$$e_2/e_0 = (k^{\text{FW}})^2/12, \quad (41)$$

$$D_i^{\text{FWHM}} = 2\sqrt{12} \frac{1}{k^{\text{FW}}} = \frac{2\sqrt{3}}{\pi} \frac{1}{\sigma^{\text{FW}}} \approx \frac{1.1}{\sigma^{\text{FW}}}. \quad (42)$$

This results in a package length of $D_i^{\text{FWHM}} = 14 \mu\text{m}$ if applied to a full K band width of $\sigma^{\text{FW}} \approx 800 \text{ cm}^{-1} = 8 \times 10^4 \text{ m}^{-1}$, for example. Eq. (42) is the uncertainty relation for the Fourier-conjugated variables σ and D_i in the specific case of a boxcar spectrum.

2. Definition

Note that the variable

$$\bar{\lambda} = \frac{\int e(\lambda)\lambda d\lambda}{\int e(\lambda) d\lambda} \quad (43)$$

is *not* used and that $\bar{\lambda} \neq 2\pi/\bar{k}$ because $\lambda = 2\pi/k$ means $d\lambda/\lambda = -dk/k$ but $\lambda d\lambda \neq -kdk$ [35]. The relation is

$$\begin{aligned} \bar{\lambda} &= 2\pi \frac{\int \frac{e(k)}{k^3} dk}{\int \frac{e(k)}{k^2} dk} = \frac{2\pi}{\bar{k}} \frac{1 - \frac{3}{k} \frac{e_1}{e_0} + \frac{6}{k^2} \frac{e_2}{e_0} + \dots}{1 - \frac{2}{k} \frac{e_1}{e_0} + \frac{3}{k^2} \frac{e_2}{e_0} + \dots} \\ &= \frac{1}{\bar{\sigma}} \left(1 - \frac{1}{k} \frac{e_1}{e_0} + \frac{3}{k^2} \frac{e_2}{e_0} + \dots \right), \end{aligned} \quad (44)$$

which means with (38) that $\bar{\lambda} > 1/\bar{\sigma}$ since e_2 and e_0 are moments of even order and positive, and that neglect of the term $\propto e_2$ would underestimate $\bar{\sigma}$.

With the estimate (41) for a flat spectrum, the relative correction is of the order of $3e_2/(\bar{k}^2 e_0) \approx (k^{\text{FW}}/\bar{k})^2/4$, or 1/400 for a relative band width of 1/10. Confirmed numerically, erroneous use of $1/\bar{\lambda}$ for $\bar{\sigma}$ yields values that are typically 11 cm^{-1} off the correct $\bar{\sigma}$ of the K band center pixel in our wide-band example.

C. Nonlinear Group Delay

The chirps in the envelopes are caused by linear dispersion (non-vanishing n'_g) and skew correlated spectra, i.e., non-vanishing e_3 .

The moment expansion has so far recovered the familiar equations (22) and (39) on the basis of neglecting the four terms in (34)–(35) with factors n'_g and/or e_3 . The largest term of these is the one $S \propto e_2$. Besides increasing the amplitude of A [25, 26, 44], it only has a tiny effect on the location of the maximum, adding $\approx D(\frac{n'_g}{2n_g})^2 \frac{e_2}{e_0}$ to D_i . All three neglected terms $S \propto e_2$ or $S \propto e_3$ actually have negligible effect on the relocation of the envelope maximum, but the term $C \propto e_3$ *does* have an effect. As a first new result of the moment expansion we find a corrected envelope location via

$$\begin{aligned} \frac{\partial}{\partial D_i} C &= 0, \\ \therefore \frac{\partial}{\partial D_i} \left\{ [n_g D_i - D_e]^2 e_2 + [n_g D_i - D_e] n'_g D_i e_3 \right\} &= 0. \end{aligned}$$

The solution D_i to this equation slightly modifies (22),

$$D_i = \frac{D_e}{n_g} \frac{1 + \frac{1}{2} \frac{n'_g}{n_g} \frac{e_3}{e_2}}{1 + \frac{n'_g}{n_g} \frac{e_3}{e_2}} \approx \frac{D_e}{n_e}, \quad (45)$$

where an “extended” refractive index n_e emerges as

$$n_e(k) \equiv n_g(k) + \frac{e_3}{2e_2} n'_g(k). \quad (46)$$

Examples of reaching beyond the group delay approximation in this fashion are provided in Tab. III related to Fig. 10. The relative correction read from the last column is of the order of 2×10^{-9} , generating a correction to the group delay estimate of 200 nm for a 100 m delay, for example. The cases of Tab. IV show that the corrections are reduced to a quarter of these values, if the band pass is reduced to half of this width.

Star (K)	atmosphere sec z (mm)	$\bar{\sigma}$ (cm^{-1})	e_3/e_2 ($10^3/\text{m}$)	$n'_g(\bar{\sigma})$ (10^{-13} m)	$\frac{1}{2} \frac{e_3}{e_2} n'_g(\bar{\sigma})$ (10^{-9})
8000	1 1.6	4498.4	-12.8	3.2	-2.05
9000	1 1.6	4499.0	-13.2	3.2	-2.11
9000	1 3.0	4497.8	-11.9	3.2	-1.90
15000	1 3.0	4499.6	-13.0	3.2	-2.08

TABLE III: Change of some variables of the group delay correction (46) as a function of the black body temperature in the star model, air mass sec z and precipitable water vapor (PWV) of the atmospheric model, integrated over a band pass from 2.05 to 2.45 μm .

Star (K)	atmosphere sec z (mm)	$\bar{\sigma}$ (cm^{-1})	e_3/e_2 ($10^3/\text{m}$)	$n'_g(\bar{\sigma})$ (10^{-13} m)	$\frac{1}{2} \frac{e_3}{e_2} n'_g(\bar{\sigma})$ (10^{-10})
8000	1 1.6	4459.7	-3.77	3.0	-5.66
9000	1 1.6	4459.8	-3.87	3.0	-5.81
9000	1 3.0	4459.1	-3.41	3.0	-5.12
15000	1 3.0	4459.6	-3.70	3.0	-5.55

TABLE IV: Change of some variables of the group delay correction (46) as in Table III over a band pass from 2.15 to 2.35 μm (from 4255 to 4651 cm^{-1} , $\sigma^{\text{FW}} = 395 \text{cm}^{-1}$). $\bar{\sigma}$ is close to σ_{ref} of Table I such that n'_g is close to (29).

Overall, this is a more systematic and consistent approach than to correct the representative point \bar{k} in the band for star spectra within the group delay approximation [16]. All effects which change the spectrum—categories listed in Section III B—are treated on equal footing.

The group delay and the correction introduced above are only defined as some form of interpolation between the fringe peaks; they try to locate the fringe package envelope to higher precision than the scale defined by the fringe spacing [32].

V. ABCD PHASE

A. Achromatic Phase Rotation

Four values called A, B, C and D originate from adding phases of $0, \pi/2, \pi$ and $3\pi/2$ to the argument of the cosine

in Eq. (19),

$$\left. \begin{array}{l} A \\ B \\ C \\ D \end{array} \right\} = \int e(k) \left\{ 1 + \cos[n(k)kD_t - kD_e + \begin{array}{l} 0 \\ \pi/2 \\ \pi \\ 3\pi/2 \end{array} \right\} dk. \quad (47)$$

This writing adds an achromatic phase to the trigonometric function, as if an ideal reversion prism ([36, 39]) had been inserted in one of the telescope beams in front of the beam combiner to push the relative phase between the s - and p -polarized components of its fields by $\pi/2$.

We are not discussing stepping methods [5, 24, 37] which add a ladder of achromatic paths sd_i ($s = 0, 1, 2, \dots$) to D_i . The stepping adds a chirped phase $\propto snkd_i$ to the cosine of (19). In sufficiently narrow bands or when $n(k)$ has a hyperbolic shape, both types of scanning may essentially be equivalent—putting aside the question of sensitivity to the polarization of the correlated $e(k)$.

B. Moment Expansion

1. Standard Formula

We pursue the same moment expansion as in Section IV A, up to the order of e_2 ,

$$\begin{aligned} A - C &\approx 2e_0 \cos \varphi(\bar{k}) \\ &\quad - 2 \{n_g(\bar{k})D_i - D_e\} e_1 \sin \varphi(\bar{k}) \\ &\quad - \{n_g(\bar{k})D_i - D_e\}^2 e_2 \cos \varphi(\bar{k}) \\ &\quad - n'_g(\bar{k})D_i e_2 \sin \varphi(\bar{k}) + \dots, \end{aligned} \quad (48)$$

$$\begin{aligned} D - B &\approx 2e_0 \sin \varphi(\bar{k}) \\ &\quad + 2 \{n_g(\bar{k})D_i - D_e\} e_1 \cos \varphi(\bar{k}) \\ &\quad - \{n_g(\bar{k})D_i - D_e\}^2 e_2 \sin \varphi(\bar{k}) \\ &\quad + n'_g(\bar{k})D_i e_2 \cos \varphi(\bar{k}) + \dots. \end{aligned} \quad (49)$$

When the choice (39) is made again, the leading terms $\propto e_0$ dominate $A - C$ and $D - B$. The result of neglecting all other terms is known as the ABCD algorithm [11, 42, 48, 49]:

$$\tan \varphi^{\text{ABCD}}(\bar{k}) = \frac{D - B}{A - C}. \quad (50)$$

The difference to dealing only with the signal A of (36) is that the information provided in the signals B to D allows to decouple the data into fringe amplitude and phase. In the following, complementarily to the contents of section IV, we look at the reduction of this *phase tracking approach* to the value of D_e , the ultimate variable of astronomical interest.

In this sense, the construction of the mean vacuum wave vector \bar{k} of (39) selects that ray, spot or piece in

the broad band spectrum which experiences the geometric path delay D_e above the atmosphere and then the optical path delay $n(\bar{k})D_i$ on the ground such that its residual phase equals the unwrapped ABCD phase φ . (Small corrections to this statement follow in Sect. V C.) If one describes long baseline interferometry as the art of equilibrating the optical path difference nD_i on the ground to the geometric path difference D_e above the atmosphere, this is only correct for one special k inside the broad-band spectrum.

2. Delay Line Mirror Vibrations

The implicit integration over varying delays caused by mirror surface vibrations on shorter timescales than the detector integration adds explicit time-dependence to the positions D_i in the arguments of the trigonometric functions (19). On short timescales, these are to lowest order linear, $D_i \rightarrow D_i + 2vt$, where v is the velocity of the mirror surface. First-order expansion of the trigonometric function $\propto t$ yields no change because the integral over the exposure time, $-t_e/2 \leq t \leq t_e/2$, vanishes. Including the second order, the trigonometric functions are multiplied by the factor $1 - (2nkv t)^2/2$, which looks like the lowest order of the familiar exponential Strehl factor of phase variance $2nkv t$.

The integral over the time interval t_e result in a multiplication of $e(k)$ by $1 - v^2 t_e^3 k^2/6$. (Vibrations which are sensed by a metrology generate other effects [14].) Expanding this term around some \bar{k} generates a common factor for e_0 to all four ABCD values of a band; it reduces the measured visibility, but cancels when building the estimator φ^{ABCD} with (50). The change of \bar{k} and contribution to the moment e_2 , however, is one of the effects that are covered implicitly by the present analysis. (Harmonic mirror vibrations could be treated as Strehl factors [3] emulated by Bessel Functions, which we do not detail further.)

C. Nonlinear ABCD Phase

1. Wideband phase correction

If the first moment e_1 vanishes (see Section IV B 1), the system of equations (48)–(49) has the matrix-vector form

$$\begin{pmatrix} A - C \\ D - B \end{pmatrix} \equiv \begin{pmatrix} X \\ Y \end{pmatrix} = \begin{pmatrix} \cos \varphi(\bar{k}) & -\sin \varphi(\bar{k}) \\ \sin \varphi(\bar{k}) & \cos \varphi(\bar{k}) \end{pmatrix} \cdot \begin{pmatrix} 2e_0 - [n_g(\bar{k})D_i - D_e]^2 e_2 \\ n'_g(\bar{k})D_i e_2 \end{pmatrix}. \quad (51)$$

[In the interpretation of $A - C$ as the p -component and the $D - B$ as the s -component of the beams, the correction by a (small) $n'_g D_i e_2$ appears as a fake polarization.]

We multiply this equation with the inverse of the rotation matrix, introduce the dimensionless parameter

$$\zeta \equiv \frac{n'_g D_i e_2}{2e_0 - [n_g D_i - D_e]^2 e_2}, \quad (52)$$

and find, with $\tan \varphi^{\text{ABCD}} = Y/X$,

$$\tan \varphi(\bar{k}) = \frac{Y - X\zeta}{Y\zeta + X} = \frac{\tan \varphi^{\text{ABCD}} - \zeta}{1 + \zeta \tan \varphi^{\text{ABCD}}}. \quad (53)$$

Taylor expansion of the arctangent of this equation for small ζ yields the corrected phase

$$\begin{aligned} \varphi(\bar{k}) &= \varphi^{\text{ABCD}} - \arctan(\zeta) \\ &\approx \varphi^{\text{ABCD}} - \zeta + \frac{1}{3}\zeta^3 + O(\zeta^5). \end{aligned} \quad (54)$$

The sign of the correction demonstrates that the observed φ^{ABCD} is larger than the phase $\varphi(\bar{k})$ assigned to the monochromatic reduction, if $n'_g > 0$. This is expected because e_2 describes adding spectral elements symmetrically to both sides of \bar{k} , and a positive derivative n' adds a term $\propto k^2$ to the phase (20), which un-balances the otherwise symmetric weighting by e_2 in the statistics of the phase spectrum (20).

The prototypical values for the example of spectra integrated over from 4081 to 4878 cm^{-1} (2.05 to 2.45 μm) of black body temperature from 6000 to 12000 K are $e_2/e_0 \approx 4.9 \times 10^4 \text{ cm}^{-2}$ [larger than the flat spectrum estimate of (41) at $\sigma^{\text{FW}} \approx 800 \text{ cm}^{-1}$], $n'_g \approx 3.2 \times 10^{-11} \text{ cm}$ from Table III, and for $D_i = 100 \text{ m}$

$$\zeta \approx \frac{1}{2} \frac{e_2}{e_0} n'_g D_i \approx 0.008 \text{ rad}. \quad (55)$$

This phase correction of 0.008 rad equals a change in D_e of $0.008/(2\pi\bar{\sigma}) \approx 2.8 \text{ nm}$ at $\bar{\sigma} \approx 4500 \text{ cm}^{-1}$. We observe that this correction from φ^{ABCD} to $\varphi(k)$ is only 1.5 % of the one calculated for the envelope shift after (46). The wide band correction shifts the fringe envelope along the D_i abscissa; the individual fringe lobes stay almost pinned. However, this result may be deceptive since the estimate (55) of (52) assumes that the term $\frac{1}{2} \frac{[n_g D_i - D_e]^2 e_2}{e_0}$ in the denominator of (52) can be neglected. Since $e_2/(2e_0) \approx 2/(D_i^{\text{FWHM}})^2$ as estimated in Section IV B 1, this assumption is only valid if the tracking settles D_i close to the envelope maximum, at $n_g D_i - D_e \approx 0$. Tracking a distance of $\frac{1}{2} D_i^{\text{FWHM}}$ away from the maximum, $\frac{1}{2} \frac{[n_g D_i - D_e]^2 e_2}{e_0}$ is approximately $\frac{1}{2}$, and ζ in (55) grows by a factor of 2, for example. So precise spectrum correction in the phase tracking needs some sort of group tracking assistance to produce the estimator of $n_g D_i - D_e$ to feed the estimation of ζ ; if the expansion (54) breaks down because the correction ζ becomes too large, one must turn to a self-consistent solution of (52) and (53) where ζ and $\varphi(\bar{k})$ are both functions of the unknown D_e .

2. Imprecise Spectra

A further source of systematic error is that \bar{k} (the effective star color) is not known exactly but only with an error $\Delta\bar{k}$, which creates a residual $e_1 \approx e_0 \Delta\bar{k}$. The terms $\propto e_1$ in $D - B$ and $A - C$ do not vanish exactly, and (48)–(49) become

$$\begin{aligned} X &= 2e_0 \cos \varphi(\bar{k}) - 2e_0 \Delta\bar{k} [n_g D_i - D_e] \sin \varphi(\bar{k}) + \dots, \\ Y &= 2e_0 \sin \varphi(\bar{k}) + 2e_0 \Delta\bar{k} [n_g D_i - D_e] \cos \varphi(\bar{k}) + \dots. \end{aligned}$$

The format still fits into (51) if we replace $n'_g D_i e_2 \rightsquigarrow n'_g D_i e_2 + 2e_0 \Delta\bar{k} (n_g D_i - D_e)$. The induced correction in the phase (55) is

$$\Delta\zeta \approx \Delta\bar{k} (n_g D_i - D_e). \quad (56)$$

Assuming again phase tracking allowing some ambiguity in the “best” lobe (“fringe jumps”), $n_g D_i - D_e$ will be of the order of 2λ , approximately $4 \times 10^{-4} \text{ cm}$ in the K band. The required $\Delta k < \Delta\zeta/(n_g D_i - D_e)$ follows from an allowable error $\Delta\zeta$ in the phase: a 10 % error in the phase, $\Delta\zeta = 0.63 \text{ rad}$, would admit an error of $\Delta\bar{k} \approx \frac{0.63}{2\lambda} \approx \frac{0.63}{4 \times 10^{-4} \text{ cm}}$, which is $\Delta\bar{\sigma} \approx 250 \text{ cm}^{-1}$. This is a quarter of the full band width and therefore easily met.

So on behalf of this particular wide-band correction to the ABCD phase, knowledge of the mean momentum number \bar{k} is not a concern; the role of \bar{k} in selecting $n(\bar{k})$ is a different theme and turns out to impose stronger error bounds on \bar{k} , as we shall see in Section VI.

VI. ASTROMETRIC APPLICATION

A. Data Reduction

If the fringe tracker locates the fringe package maximum, the data reduction converts the delay line mirror position D_i at that point into $D_e = n_e(\bar{k}) D_i$ of (45). If the tracker senses the ABCD phase, the data reduction applies the correction (54) and reduces (19) to

$$D_e = n(\bar{k}) D_i - \frac{\varphi(\bar{k})}{\bar{k}} \quad (57)$$

of (20). The task of disentangling the two terms in the cosine of (19) is a key difference between an astrometric data analysis and a fringe tracker.

In both cases, the delay line positions D_i are probably obtained from an auxiliary metrology system (which we did not address), and in both cases of the product $n_{(e)}(\bar{k}) D_i$ enters the metrology reading such that it reduces the errors if the metrology is already operating close to \bar{k} . A mixed/hybrid operation of both methods is useful. The common well-known problem of both approaches is the fluctuation of \bar{k} as a function of the spectral shape of $e(k)$, which enters the data reduction directly as \bar{k} or indirectly as $n_e(\bar{k})$, which we discuss in the final subsections.

B. Unknown Star Temperature

1. Sensitivity

This well-known hybrid sensitivity of the central \bar{k} to the spectral width and star color is estimated in Tab. V. Naïve scaling of the sensitivity proportional to the inverse squared width of the spectral channel turns out to be quite inaccurate.

λ range (μm)	$\bar{\sigma}$ (8000 K)	$\Delta\bar{\sigma}$ (\rightsquigarrow 9000 K)
2.05 – 2.45	4498.0	0.656
2.05 – 2.26	4657.0	0.215
2.26 – 2.45	4256.8	0.121
2.05 – 2.19	4724.7	0.102
2.19 – 2.32	4440.2	0.068
2.32 – 2.45	4197.6	0.054
2.05 – 2.15	4766.0	0.054
2.15 – 2.25	4549.0	0.045
2.25 – 2.35	4350.9	0.037
2.35 – 2.45	4169.4	0.031

TABLE V: The sensitivity of the pivot wave number $\bar{\sigma}$ to a change of the temperature of a pure black-body spectrum for different spectral resolution (subdivisions) of the K band. In accordance with Fig. 4, the mean wave number shifts to higher values for the increase from 8000 to 9000 K.

Since Fig. 13 will show that the curves become flatter at higher temperatures, the example at 8000 K is already some worst case.

2. Phase Tracking

The astrometric use of these results would concentrate on the estimate of D_e and derive it from the measured phase via (57). The “direct scaling” error in φ/\bar{k} from a poorly known star temperature T is the first order differential

$$\Delta D_e \approx \frac{\varphi}{\bar{k}^2} \Delta \bar{k} = \frac{\varphi/(2\pi)}{\bar{\sigma}^2} \frac{\partial \bar{\sigma}}{\partial T} \Delta T. \quad (58)$$

The term $\frac{\partial \bar{\sigma}}{\partial T} \Delta T$ would be of the order of 0.7 cm^{-1} for an error $\Delta T \approx 1000 \text{ K}$, see the first line in Table V. At 100 m of delay, the term $\varphi/(2\pi)$ would be ≈ -29 cycles, see the lower graph in Fig. 9. Using in addition $\bar{\sigma} \approx 4500 \text{ cm}^{-1}$, the “direct scaling” error (58) is $\Delta D_e \approx -10 \text{ nm}$.

3. Group Delay Tracking

If the data reduction uses (45) with (46), the precise value of \bar{k} determines where on the humid air dispersion curve n has to be read. Since \bar{k} represents a spectrum, the number of spectral channels to represent the band takes

influence on this knowledge of the differential index of refraction, as a higher number of spectral channels means less sensitivity to the star colors—this is essentially the same result as from comparison of Figs. 12 and 13 in [35]. Each change of $\bar{\sigma}$ by 1 cm^{-1} induces a change of n by 1.1×10^{-10} , see c_{lref} of Table I. With the same error in $\bar{\sigma} \approx 0.7 \text{ cm}^{-1}$ derived from $\Delta T \approx 1000 \text{ K}$ as in the previous subsection, the error in n reaches $\approx 8 \times 10^{-11}$, which is $+8 \text{ nm}$ of “indirect” error per 100 m of delay.

This sensitivity to a change in $\bar{\sigma}$ induced by a change in the star color is practically the same as in the previous section with the “Phase Tracking” reduction. [This is no coincidence. The condition (21) actually sets up φ to mediate this scaling: Consider the derivative $\frac{\partial(\varphi/\sigma)}{\partial\sigma} = \frac{\partial\varphi/\partial\sigma}{\sigma} - \frac{\varphi}{\sigma^2}$ which becomes $-\frac{\varphi}{\sigma^2}$ via (21). Using (20), the derivative can also be written $2\pi \frac{\partial(nD_i - D_e)}{\partial\sigma} \approx 2\pi D_i \frac{\partial n}{\partial\sigma}$. This allows the substitution $\frac{\varphi/(2\pi)}{\sigma^2} \rightsquigarrow -D_i \frac{\partial n}{\partial\sigma}$ in (58) to prove equivalence of both error propagations.]

C. Varying Air Mass and PWV

The influence of variations in the precipitable water vapor (PWV) and air mass on the mean wave number in the spectral channels is investigated by considering Fig. 5 for water vapor columns of 1, 1.6 and 3 mm, and for air masses of 1 and 1.5. (See [15] for a discussion of water vapor absorption in the infrared.)

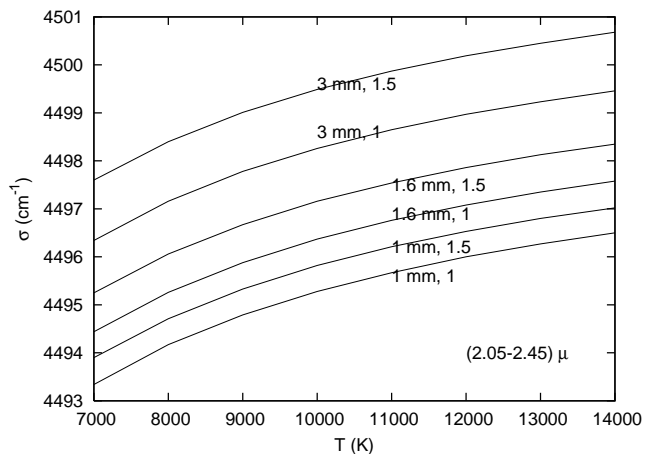


FIG. 13: Black body spectra from 7000 to 14000 K multiplied with the air transmission spectrum for 6 pairs of PWV and air mass and multiplied with the detector quantum efficiency define these effective wave numbers in the 2.05–2.45 μm band according to (39).

Black body spectra from $1.52 \mu\text{m}$ to $2.78 \mu\text{m}$ have been sliced into 20000 virtual sub-channels, multiplied by the air transmission factors and with the detector response of Fig. 6 to yield representations $e(k)$ as in Fig. 7. Summation of (39) over sub-channels creates Figs. 13 and 14. The flatter lines in Fig. 14 show that the vari-

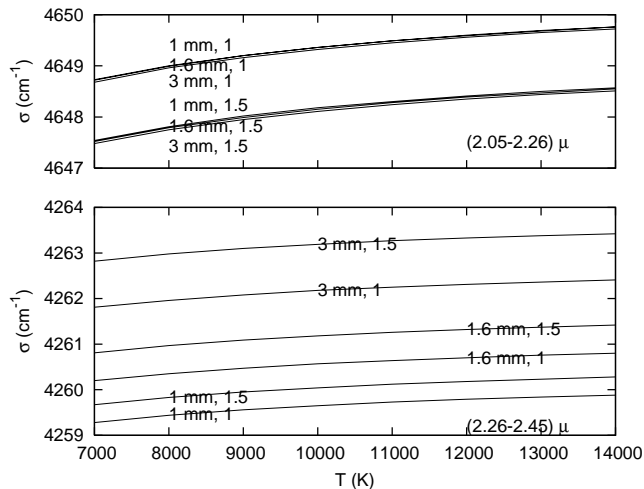


FIG. 14: The wide band of Fig. 13 is split into two bands from 2.05 to 2.26 μm and from 2.26 to 2.45 μm , leading to these new central wave numbers $\bar{\sigma}$ as a function of star temperature, PWV and air mass.

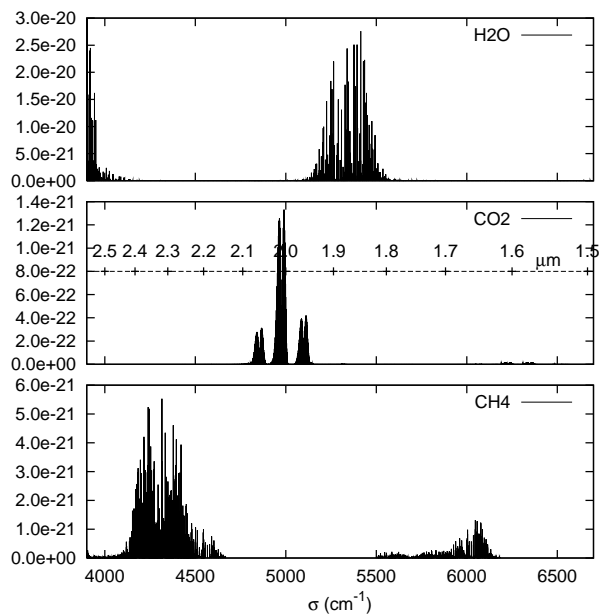


FIG. 15: Line strengths of important atmospheric gases (water, carbon dioxide, methane) in units of $\text{cm}^{-1}/(\text{molecule cm}^{-1})$, contributing to Fig. 7 [41].

ation of the central \bar{k} as a function of the black body temperature is reduced efficiently if the band width is reduced—consistent with the calculations on pure black body spectra of Table V.

The air mass controls the strength of the CO_2 absorption bands near 4850 cm^{-1} , and the PWV controls the termination of the atmospheric window near 4200 cm^{-1} (Fig. 15). Their asymmetric position in opposite corners in the two bands explains the opposite signs of the gradients of $\bar{\sigma}$ with respect to these two parameters in the two plots of Fig. 14. For this reason, splitting the original wide band does not desensitize $\bar{\sigma}$ from the sky transmission parameters as easily as from the broad star spectra.

VII. SUMMARY

The effect of air dispersion on visibilities measured by two-beam astronomical interferometers is accompanied by effects of astrometric signature: Accumulation of dispersed phases over correlated wide-band spectra relocates the maximum of the wave packet envelope as if the group refractive index n_g had been replaced by an extended refractive index n_e which equals the group refractive index n_g augmented by a hybrid product between some spectral skewness and the dispersion $\partial n_g / \partial k$ of the group refractive index. The complementary influence on the phase calculated with the ABCD formula is typically much smaller.

Not only the star spectrum but also the (variable) atmospheric conditions and other instrumental effects shape the source spectrum and play important roles in determining pivot wave-numbers of the spectral bands.

Acknowledgments

This work is supported by the NWO VICI grant of 15-6-2003 “Optical Interferometry: A new Method for Studies of Extrasolar Planets” to A. Quirrenbach.

-
- [1] Abramowitz, M., and I. A. Stegun (eds.), 1972, *Handbook of Mathematical Functions* (Dover Publications, New York), 9th edition, ISBN 0-486-61272-4.
 - [2] Ait-Ameur, K., and F. Sanchez, 2004, *Opt. Commun.* **233**(1–3), 39.
 - [3] Altarac, S., P. Berlioz-Arthaud, E. Thiébaud, R. Foy, Y. Y. Balega, J. C. Dainty, and J. J. Fuensalida, 2001, *Month. Not. Roy. Astron. Soc.* **322**(1), 141.
 - [4] Åslund, M., S. D. Jackson, J. Canning, A. Teixeira, and K. Lyytikäinen-Digweed, 2006, *Opt. Commun.* **262**(1), 77.
 - [5] Basden, A. G., and D. F. Buscher, 2005, *Month. Not. Roy. Astron. Soc.* **357**(2), 656.
 - [6] Berger, D. H., T. A. ten Brummelaar, W. G. Gagnuolo, and H. A. McAlister, 2003, in *Interferometry for Optical Astronomy II*, edited by W. A. Traub (Int. Soc. Optical

- Engineering), volume 4838 of *Proc. SPIE*, pp. 974–982.
- [7] Boden, A. F., 2000, in *Principles of Long Baseline Stellar Interferometry*, edited by P. R. Lawson (National Aeronautics and Space Administration), p. 9, JPL publication 00-009 07/00.
- [8] Boehm, J., and H. Schuh, 2003, in *16th Working Meeting on European VLBI for Geodesy and Astrometry*, edited by W. Schwegmann and V. Thorandt (Bundesamt für Kartographie und Geodäsie), volume 16, pp. 131–143.
- [9] Born, M., and E. Wolf, 1999, *Principles of Optics* (Cambridge University Press, Cambridge), 7th edition.
- [10] Brachet, F., 2005, *Étude et développement d'un déphaseur achromatique pour l'interférométrie en frange noire*, Ph.D. thesis, l'Université de Paris-Sud (XI).
- [11] Cai, L.-Z., Q. Liu, Y.-R. Wang, X.-F. Meng, and M.-Z. He, 2006, *Appl. Opt.* **45**(6), 1193.
- [12] Ciddor, P. E., and R. J. Hill, 1999, *Appl. Opt.* **38**(9), 1663.
- [13] Colavita, M. M., M. R. Swain, R. L. Akeson, C. D. Koresko, and R. J. Hill, 2004, *Publ. Astron. Soc. Pac.* **116**(823), 876.
- [14] Comolli, L., and B. Saggin, 2005, *Rev. Sci. Instr.* **76**(12), 123112.
- [15] Cormier, J. G., J. T. Hodges, and J. R. Drummond, 2005, *J. Chem. Phys.* **122**(11), 114309.
- [16] Daigne, G., and J.-F. Lestrade, 1999, *Astron. Astrophys. Suppl.* **138**(2), 355.
- [17] Gandhi, P., C. S. Crawford, and A. C. Fabian, 2002, *Month. Not. Roy. Astron. Soc.* **337**(3), 781.
- [18] Greisen, E. W., M. R. Calabretta, F. G. Valdes, and S. L. Allen, 2006, *Astron. & Astrophys.* **446**(2), 747.
- [19] Haruna, M., M. Ohmi, T. Mitsuyama, H. Tajiri, H. Maruyama, and M. Hashimoto, 1998, *Opt. Lett.* **23**(12), 966.
- [20] Heraeus Quarzglas, 2003, *Quarzglas für die Optik, Daten und Eigenschaften*, Technical Report, URL <http://www.heraeus-quarzglas.com>.
- [21] Hill, R. J., S. F. Clifford, and R. S. Lawrence, 1980, *J. Opt. Soc. Am.* **70**(10), 1192.
- [22] Hill, R. J., and R. S. Lawrence, 1986, *Infrared Phys.* **26**(6), 371.
- [23] Iserles, A., and S. Nørsett, 2005, *Proc. R. Soc. A* **461**(2057), 1383.
- [24] Jaffe, W. J., 2004, in *Astronomical Telescopes and Instrumentation*, edited by W. A. Traub (Int. Soc. Optical Engineering), volume 5491 of *Proc. SPIE*, pp. 715–725.
- [25] Lawson, P. R., 1996, *Appl. Opt.* **35**(25), 5122.
- [26] Lévêque, S., B. Koehler, and O. von der Lühse, 1996, *Astrophys. Space Science* **239**(2), 305.
- [27] Lord, S. D., 1992, *A New software tool for computing earth's atmospheric transmission of near- and far-infrared radiation*, NASA Technical Memorandum 103957, NASA, URL <http://www.gemini.edu/sciops/ObsProcess/obsConstraints/ocTr>
- [28] Mathar, R. J., 1998, *Am. J. Phys.* **66**(8), 659.
- [29] Mathar, R. J., 2004, arXiv:astro-ph/0411384 .
- [30] Mathar, R. J., 2004, *Appl. Opt.* **43**(4), 928.
- [31] Mathar, R. J., 2005, *Baltic Astronomy* **14**(2), 277.
- [32] Meisner, J. A., 2001, in *From optical to millimeter interferometry: scientific and technological challenges*, edited by J. Surdej, J. P. Swings, D. Caro, and A. Detal (Institut d'Astrophysique et de Geophysique), volume 36 of *Int. Astrophys. Coll.*, pp. 225–231.
- [33] Meisner, J. A., and R. S. Le Poole, 2003, in *Interferometry for Optical Astronomy II*, edited by W. A. Traub (Int. Soc. Optical Engineering), volume 4838 of *Proc. SPIE*, pp. 609–624.
- [34] Meisner, J. A., R. N. Tubbs, and W. J. Jaffe, 2004, in *New Frontiers in Stellar Interferometry*, edited by W. A. Traub (Int. Soc. Optical Engineering), volume 5491 of *Proc. SPIE*, pp. 725–740.
- [35] Milman, M. H., 2005, *J. Opt. Soc. Am. A* **22**(12), 2774.
- [36] Moreno, I., 2004, *Appl. Opt.* **43**(17), 3373.
- [37] Padilla, C. E., V. I. Karlov, L. K. Matson, K. Soosaar, and T. ten Brummelaar, 1998, in *Astronomical Interferometry*, edited by R. D. Reasenberg (Int. Soc. Optical Engineering, Kona), volume 3350 of *Proc. SPIE*, pp. 1045–1056.
- [38] Pavliček, P., and J. Soubusta, 2004, *Appl. Opt.* **43**(4), 766.
- [39] Pegis, R. J., and M. M. Rao, 1963, *Appl. Opt.* **2**(12), 1271.
- [40] Pu, J., 1993, *J. Optics (Paris)* **24**(3), 141.
- [41] Rothman, L. S., A. Barbe, D. C. Benner, L. R. Brown, C. Camy-Peyret, M. R. Carleer, K. Chance, C. Clerbaux, V. Dana, V. M. Devi, A. Fayt, J.-M. Flaud, *et al.*, 2003, *J. Quant. Spectrosc. Radiat. Transfer* **82**, 5.
- [42] Shao, M., and D. H. Staelin, 1977, *J. Opt. Soc. Am.* **67**(1), 81.
- [43] Stubbs, C. W., and J. L. Tonry, 2006, *Astrophys. J.* **646**, 1436.
- [44] Tango, W. J., 1990, *Appl. Opt.* **29**(4), 516.
- [45] ten Brummelaar, T. A., 1995, *Appl. Opt.* **34**(13), 2214.
- [46] Tubbs, R. N., J. A. Meisner, E. J. Bakker, and S. Albrecht, 2004, in *Astronomical Telescopes and Instrumentation*, edited by W. A. Traub (Int. Soc. Optical Engineering), volume 5491 of *Proc. SPIE*, pp. 588–599.
- [47] Turyshev, S. G., 2003, *Appl. Opt.* **42**(1), 71.
- [48] Wyant, J. C., 1975, *Appl. Opt.* **14**(12), 2622.
- [49] Zhong, X., 2006, *J. Opt. A: Pure Appl. Opt.* **8**(3), 300.